IEEE Access
Multidisciplinary ⋮ Rapid Review ⋮ Open Access Journal

Received October 26, 2021, accepted November 4, 2021, date of publication November 11, 2021,
date of current version November 22, 2021.

Digital Object Identifier 10.1109/ACCESS.2021.3127502

Real-Time Simulator of a Six Degree-of-Freedom Hydraulic Manipulator for Pipe-Cutting Applications

MYOUNGHO KIM[1], (Member, IEEE), SUNG-UK LEE[1], (Member, IEEE), AND SUNG-SOO KIM[2]

[1]Nuclear Robot Division, Korea Atomic Energy Research Institute, Yuseong-gu, Daejeon 34057, South Korea
[2]Department of Mechatronics Engineering, Chungnam National University, Yuseong-gu, Daejeon 34134, South Korea

Corresponding author: Sung-Uk Lee (sulee@kaeri.re.kr)

This work was supported by the Korea Institute of Energy Technology Evaluation and Planning (KETEP) funded by the Ministry of Trade, Industry, and Energy (MOTIE) (Development of a remote dismantling training system with force-torque responding virtual nuclear power plant) under Grant 20201510300280.

ABSTRACT Hydraulic manipulators exhibit significant potential for various applications owing to their advantages. To simulate scenarios and evaluate their control performance effectively, a real-time simulation method of hydraulic manipulators is required. Simulations are easier and safer to conduct, and are therefore preferred over physical experiments. This paper discusses a real-time simulator for hydraulic manipulators. This simulator entails servo valve dynamics, hydraulic equations, a friction model, a pipe-cutting model, mechanical manipulator dynamics, a robust numerical integration algorithm, and a controller. The hydraulic manipulator dynamics was developed by considering the compressibility of fluid and applying the multibody recursive formula to effectively implement the characteristics of the actual system. In addition, a non-iterative HHT-α numerical integration algorithm was applied to real-time simulations including the stiff characteristics of the hydraulic system and the cutting force. The performance of the real-time simulator was verified by comparing the results obtained with the results of the open-loop control experiment. The results of circular trajectory-tracking and pipe-cutting simulations showed that an advanced simulation with a controller can be realized in a working environment, and the real-time performance was verified by measuring the computational time.

INDEX TERMS Control simulation, hydraulic manipulator, pipe-cutting, real-time simulator, real-time integration algorithm.

I. INTRODUCTION

Hydraulic manipulators have been applied to underwater manipulation, academic research, building maintenance, and dismantling [1]–[5]. For example, hydraulic manipulators are used in decommissioning of nuclear power plants to cut contaminated pipes or core facilities, which are large and heavy [5], [6]. The hydraulic system can obtain a large force/torque with a small input and has robustness for overload. Thus, hydraulic manipulators have a high ratio of power to weight than electric manipulators and can be more compact for manipulation. Therefore, hydraulic manipulators are still considered for robot systems that manipulate heavy objects or require high force/torque.

The associate editor coordinating the review of this manuscript and approving it for publication was Tao Wang.

Experiments should be repeated several times to stably use hydraulic manipulators because various problems are resolved based on feedback information. However, physical experiments have limitations in terms of stability, cost, and time. Owing to Industry 4.0, digital twins have been receiving more attention than physical experiments [7]–[9]. Real-time simulation of the digital twin is effective not only in representing physical environments, but also in integrating with real-time data, optimizing design, and enhancing system performance. Therefore, real-time simulations are necessary for system design, development of control systems, and operator training of hydraulic manipulators [6].

Recently, various simulators have been proposed for the simulation of robot systems [10]. These simulators provide several functions such as virtual sensors, working environments, kinematics, and dynamics. However, simulating

hydraulic manipulators is complex because most simulators can not include hydraulic actuator systems. Thus, further studies on real-time simulation of hydraulic manipulators are required.

Previous research related to the simulation of hydraulic manipulators has shown that real-time simulation can be performed using the simplification of hydraulic equations [11]–[13]. They increased the computational efficiency by neglecting the compressibility of the fluid to ensure real-time performance because highly accurate models cannot be simulated in real-time. However, the accuracy of the simulation was decreased due to the simplified model, and only a simple target system with less than three degrees-of-freedom (DOF) was considered. Thus, a more accurate and efficient method is required to simulate the hydraulic manipulator with multi DOF in real-time.

Real-time simulations of hydraulic manipulators with improved accuracy have also been presented [14]–[17]. The friction model and compressibility of the fluid were considered to enhance the accuracy of simulations. The real-time performance was satisfied using a hybrid model, which mixed simplified and detailed models, or screw theory. These studied focused on a more accurate and efficient modeling method to increase simulation speed and accuracy, and real-time simulations of multi DOF hydraulic manipulators were used for verification. However, only the motion simulations according to the predefined input were performed. The working environment such as the contact model should be considered to simulate the working scenarios.

Real-time simulations including contact model were conducted [18]. This study combined a mechanical system, hydraulic actuator, and contact modeling methods in real-time simulations. Real-time performance was achieved while maintaining accuracy using a recursive formula-based modeling method and a penalty method-based contact model. These methods were applied to a hydraulic harvester, and real-time simulation was possible for the actual working scenarios.

However, most of the previous studies did not consider integration with real-time data such as the controller. The evaluation of the control system is also important for operating hydraulic manipulators. Moreover, simulations of the cutting process are not possible. Previous studies only addressed collision detection and could not obtain real-time simulations. Therefore, this study proposed a real-time simulator for hydraulic manipulators capable of advanced simulations that include the controller and cutting environment.

A robust numerical integration algorithm is also required for advanced simulation in real-time because it is essential to obtain a stable solution for real-time data or contact conditions. Generally, explicit integration algorithms are widely used in the simulation, such as Runge-Kutta or Adams-Bashforth methods [19]. These methods can be easily implemented due to simple formulas. However, explicit integration algorithms are not suitable for real-time simulation of hydraulic manipulators because the hydraulic system becomes a stiff system due to the compressibility of the fluid. Thus, implicit integration algorithms are required to obtain a stable solution for the stiff system.

The implicit integration algorithm based on the backward Euler method is proposed for the real-time simulation of stiff systems [20]–[22]. This method can maintain the accuracy of the solution even though the integral step size is larger than explicit integration algorithms. The simulation speed can be increased, but the accuracy of the solution is significantly decreased for a highly stiff system. A real-time simulation using the Hilber-Hughes-Taylor-α (HHT-α) method was presented to increase the accuracy of solutions [23]–[25]. This method can simulate highly stiff systems in real-time by adding a numerical damping effect; further, the accuracy of its solution is better than that of the backward Euler method solution. Thus, the HHT-α method is effective for the real-time simulation of the hydraulic manipulator. However, an iterative method is required to apply the HHT-α method. Implementing the iterative method for real-time simulations is difficult because the same computation efficiency should be guaranteed for every integral step. The fixed number of iterations to obtain a stable solution requires several repeated simulations. Therefore, a noniterative implicit integration algorithm is necessary.

Thus, this study proposes a real-time simulator of a six DOF hydraulic manipulator for pipe-cutting applications. It combined a hydraulic actuator model, friction model, mechanical manipulator model, pipe-cutting model, and controller. For the hydraulic actuator model, servo valve dynamics and compressibility of the fluid were considered to represent the actual environment. The mechanical manipulator system was modeled using the multibody recursive formula [26] to increase the computational efficiency, and the modified LuGre friction model [27] was applied. The accuracy of the hydraulic manipulator model was verified via a comparison with the open-loop control experiment. In addition, a noniterative HHT-α method [28], which is a robust numerical integration algorithm without the iterative method, was applied to guarantee real-time performance. A proportional-integral-differential (PID) controller with a systematic gain selection method [29] was considered to simulate the position control of the hydraulic manipulator's end-effector. The pipe-cutting model assumed a situation wherein a circular saw installed on hydraulic manipulator cuts the pipe along the cutting trajectory. Finally, the performance of the developed real-time simulator model was verified through circular trajectory-tracking and pipe-cutting simulation, and real-time capability was confirmed by measuring the central processing unit (CPU) time required for computations. The contributions of this study are as follows:

- To propose a real-time simulator of the hydraulic manipulator with a controller for a pipe-cutting environment.
- To provide real-time performance using a noniterative HHT-α numerical integration algorithm.
- To validate the developed model through real-time simulations of the hydraulic manipulator.

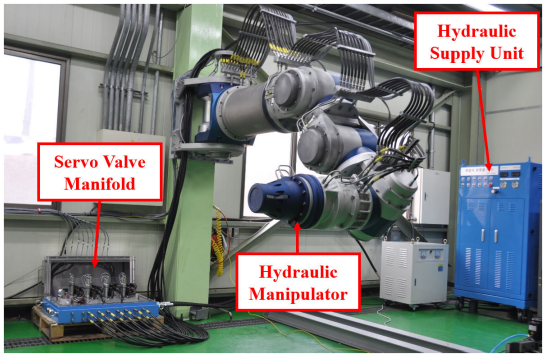

FIGURE 1. Six DOF hydraulic manipulator.

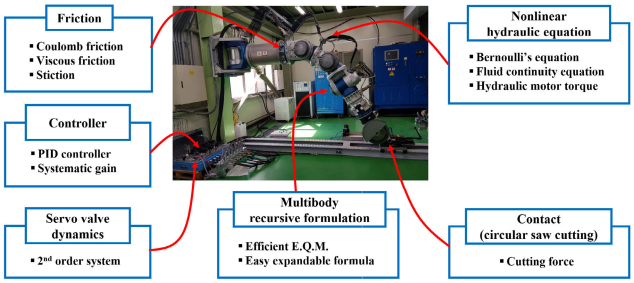

FIGURE 2. Structure of the hydraulic manipulator dynamics.

TABLE 1. Modified D-H parameters and ranges of the hydraulic manipulator.

Axis	α_{i-1}	a_{i-1}	d_i	θ_i	Range
1	0	0	0	θ_1	$\pm\pi/2$
2	$-\pi/2$	0	$1.329 + d_2$	$-\pi/2$	0-0.4 m
3	$-\pi/2$	0	0	$\theta_3 - \pi/2$	$\pm\pi/2$
4	0	0.502	0	θ_4	$\pm\pi/2$
5	$-\pi/2$	0.482	0	$\theta_5 - \pi/2$	$\pm\pi/2$
6	$-\pi/2$	0	0.9291	θ_6	$\pm\pi$

II. HYDRAULIC MANIPULATOR

The hydraulic manipulator [30] was designed with six DOF and an R-P-R-R-R-R structure, as shown in Fig. 1. It was developed for use in decommissioning of core facilities in nuclear power plants such as reactors, steam generators, and pressurizers. Modified Denavit-Hartenberg (D-H) parameters and ranges are listed in Table 1. The payload is 250 kg and the maximum extension reach is 3.2 m. All joints are actuated using Danfoss hydraulic gerotor motors and Star servo valves. The detailed specifications are summarized in Tables 2 and 3. A harmonic reducer was applied to revolute joints to increase the accuracy of position, and a ball screw mechanism was used to convert rotational motion into linear motion at the second joint. Moreover, a module type was applied for easy maintenance or expansion.

The dynamics of hydraulic manipulator entails servo valve dynamics, hydraulic equations with the compressibility of fluid, mechanical manipulator dynamics, a friction model, and a pipe-cutting model, as shown in Fig. 2.

TABLE 2. Specifications of hydraulic actuators.

	1, 3, and 4 axes	2, 5 and 6 axes
Hydraulic motor	Danfoss OMP80 (gerotor type)	Danfoss OMM40 (gerotor type)
Max. speed	960 rpm	630 rpm
Max. torque	150 N·m	45 N·m
Max. pressure drop	140 bar	90 bar
Mechanical parts	Harmonic reducer (1:160)	Harmonic reducer (1:160)
		Ball screw mechanism (5 mm/rev)

TABLE 3. Specifications of servo valves.

	1, 3, and 4 axes	2, 5, and 6 axes
Servo valve	Star ST-456 (Nozzle-flapper type)	Star ST-454 (Nozzle-flapper type)
Max. flow rate	55 lpm	20 lpm
Max. operating pressure	315 bar	315 bar
Max. rated input	±20 mA	±20 mA

A. SERVO VALVE DYNAMICS

We consider a second-order system for the servo valve to apply the actual dynamic characteristic as follows:

$$\ddot{x}_v^i(t) + 2\zeta_v\omega_{n_v}\dot{x}_v^i(t) + \omega_{n_v}^2 x_v^i(t) = \omega_{n_v}^2 K_{sv}^i u^i(t), \tag{1}$$

where $i = 1, 2, \cdots, 6$ is the index of each servo valve, t is the index of the time, x_v is a displacement of spool, K_{sv} is a valve gain, u is a control input current, and ζ_v and ω_{n_v} are damping ratio and natural frequency.

The damping ratio and natural frequency can be obtained from the datasheet. Then, the spool displacement of the servo valve according to the control input can be computed through (1), and the flow rate supplied to the hydraulic motors can be controlled.

B. HYDRAULIC EQUATIONS

The hydraulic equations can be defined through Bernoulli's and fluid continuity equations [31]. The flow rate at the supply and return ports of the hydraulic motor can be defined using Bernoulli's equation as follows:

$$Q_1^i(t) = \begin{cases} C_d^i x_v^i(t)\sqrt{P_s - P_1^i(t)} & \text{if } x_v^i(t) \geq 0 \\ C_d^i x_v^i(t)\sqrt{P_1^i(t)} & \text{otherwise,} \end{cases}$$

$$Q_2^i(t) = \begin{cases} -C_d^i x_v^i(t)\sqrt{P_2^i(t)} & \text{if } x_v(t) \geq 0 \\ -C_d^i x_v^i(t)\sqrt{P_s - P_2^i(t)} & \text{otherwise,} \end{cases}$$

$$Q_{leak}^i(t) = \begin{cases} C_{in}^i\sqrt{P_1^i(t) - P_2^i(t)} & \text{if } x_v^i(t) \geq 0 \\ -C_{in}^i\sqrt{P_2^i(t) - P_1^i(t)} & \text{otherwise,} \end{cases} \tag{2}$$

where Q_1 and Q_2 are flow rates of the supply and return ports, respectively; Q_{leak} is a internal leak; P_s is a pressure supplied from the hydraulic supply unit; P_1 and P_2 are pressure of the supply and return ports, respectively; C_d is the flow coefficient; and C_{in} is the internal leakage coefficient.

Moreover, the pressure at the supply and return ports of the hydraulic motor can be obtained from the fluid continuity equation as follows:

$$\begin{aligned}\dot{V}_1^i(t) &= D_m^i \dot{\theta}_m^i(t) = -\dot{V}_2^i(t),\\ \dot{P}_1^i(t) &= \frac{\beta_e}{V_1^i(t)}\left[Q_1^i(t) - Q_{leak}^i(t) - \dot{V}_1^i(t)\right],\\ \dot{P}_2^i(t) &= \frac{\beta_e}{V_2^i(t)}\left[Q_2^i(t) + Q_{leak}^i(t) - \dot{V}_2^i(t)\right],\end{aligned} \tag{3}$$

where V_1 and V_2 are the total volume of the supply and return ports, including horse, respectively; D_m is the volumetric displacement of the hydraulic motor; $\dot{\theta}_m$ is the angular velocity of the hydraulic motor; and β_e is the fluid bulk modulus.

The hydraulic motor torque according to the control input can be obtained using (1), (2), and (3) as follows:

$$\tau_m^i(t) = \eta_m^i \eta_g^i \frac{D_m^i\left[P_1^i(t) - P_2^i(t)\right]}{2\pi}, \tag{4}$$

where τ_m is a hydraulic motor torque, η_m is the mechanical efficiency, and η_g is the gear ratio.

Consequently, the hydraulic motor torque that includes both the servo valve dynamics and the compressibility of the fluid can be implemented. The parameters for the analysis of the hydraulic system were obtained through actual experiments.

C. FRICTION MODEL

A friction model was applied to represent the friction of each joint for the hydraulic manipulator. We considered a modified LuGre friction model [27] to satisfy both efficiency and accuracy. This model includes Coulomb friction, viscous friction, stiction, and Stribeck effect. The detailed expression is as follows:

$$\begin{aligned}\dot{z}^j(t) &= \dot{q}^j(t) - \frac{|\dot{q}^j(t)|}{g(\dot{q}^j(t))} z^j(t),\\ g(\dot{q}^j(t)) &= \frac{1}{\sigma_0^j}\left[F_{cf}^j + \left(F_s^j - F_{cf}^j\right) e^{-(\dot{q}^j(t)/v_s^j)^2}\right],\\ Q_f^j &= \sigma_0^j z^j(t) + \sigma_1^j \dot{z}^j(t) + F_{vf}^j \dot{q}^j(t),\end{aligned} \tag{5}$$

where $j = 1, 2, \cdots, 6$ is an index of the joint, Q_f is a total friction force, z is an average deflection of the bristles, $\dot{q}(t)$ is the joint velocity, F_{cf} is the Coulomb friction, F_s is the stiction, F_{vf} is the viscous friction, v_s is the Stribeck velocity, σ_0 is the stiffness, and σ_1 is the damping ratio.

The friction parameters in (5) were selected through physical experiments.

D. PIPE-CUTTING MODEL

We considered cutting the pipe by attaching a circular saw on the hydraulic manipulator's end-effector, as shown in Fig. 3.

The teeth of the circular saw come into contact with the pipe with a cutting force. Thus, calculating the contact area and finding the teeth of the circular saw in the contact area

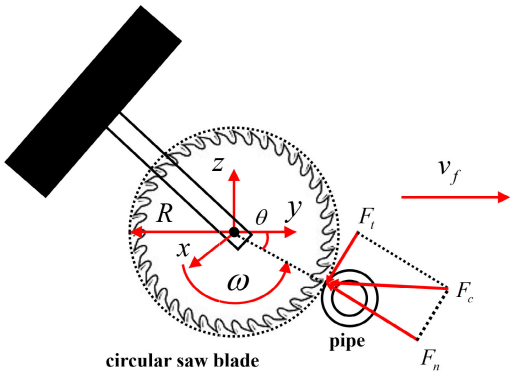

FIGURE 3. Configuration of the pipe-cutting using a circular saw.

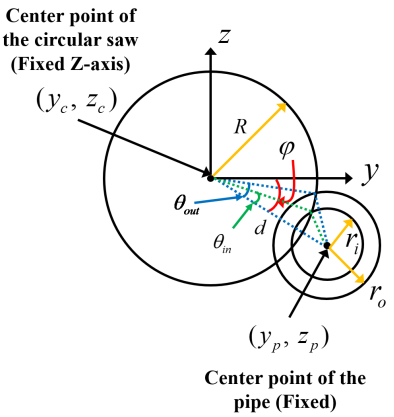

FIGURE 4. Contact area of the pipe-cutting.

are crucial. The contact area is shown in Fig. 4, and can be obtained using (6).

$$\begin{aligned}d &= \sqrt{(y_p - y_c)^2 + (z_p - z_c)^2},\\ \theta_{out} &= \text{acos}\left(\frac{d^2 + R^2 - r_o^2}{2dR}\right),\\ \theta_{in} &= \text{acos}\left(\frac{d^2 + R^2 - r_i^2}{2dR}\right),\\ \varphi &= \text{asin}\left(\frac{|z_p - z_c|}{d}\right),\end{aligned} \tag{6}$$

where d is the distance between the center point of the circular saw and the center point of the pipe, R is the radius of the circular saw, r_o is the outer radius of the pipe, and r_i is the inner radius of the pipe.

In addition, the position of each tooth considering the rotation of the circular saw can be defined as follows:

$$\begin{aligned}\theta_k(n,t) &= \frac{n2\pi}{N} + \omega t,\\ \theta_t(n,t) &= \theta_k(n,t) - \left\lfloor \frac{\theta_k(n,t)}{2\pi} \right\rfloor 2\pi,\end{aligned} \tag{7}$$

where n is the index of the tooth, $\theta_t(n,t)$ is the angle of each tooth with respect to the positive Y-axis, N is the total number

of teeth, ω is the angular velocity of the circular saw, and $\lfloor \cdot \rfloor$ is the floor function.

Whether the teeth of the circular saw are within the contact area can be detected, as follows:

$$\begin{aligned}
&\text{when } 2\pi - (\varphi + \theta_{out}) \le \theta_t(n,t) \le 2\pi - (\varphi + \theta_{in}) : \\
&\qquad\qquad N_t(n,t) = 1, \\
&\text{when } 2\pi - (\varphi - \theta_{in}) \le \theta_t(n,t) \le 2\pi - (\varphi - \theta_{out}) : \\
&\qquad\qquad N_t(n,t) = 1, \\
&\text{otherwise} : N_t(n,t) = 0,
\end{aligned} \tag{8}$$

where $N_t(n,t)$ denotes a state variable for each tooth of circular saw; and 1 means true and 0 means false.

The cutting force of each tooth can be expressed as follows [32]:

$$F_c(n,t) = N_t(n,t)\frac{\tau_s W\ 2\pi v_f \sin(\theta_t(n,t))}{\omega N \sin(\phi_s)\cos(\phi_s + \beta_f - \alpha_r)}, \tag{9}$$

where τ_s is the shear stress for the material of the pipe, W is the thickness of the circular saw, v_f is the feed rate, ϕ_s is the shear angle, β_f is the friction angle, and α_r is the rake angle. The parameters were obtained through the datasheet.

The cutting force of (9) can be divided into tangential force (F_t) and normal force (F_n) as follows, respectively:

$$\begin{aligned}
F_t(n,t) &= F_c(n,t)\cos(\beta_f - \alpha_r), \\
F_n(n,t) &= F_c(n,t)\sin(\beta_f - \alpha_r).
\end{aligned} \tag{10}$$

Finally, the contact force of pipe-cutting is expressed in Cartesian space as follows:

$$\begin{aligned}
F_y(n,t) &= F_t(n,t)\sin(\theta_t(n,t)) + F_n(n,t)\cos(\theta_t(n,t)), \\
F_z(n,t) &= F_t(n,t)\cos(\theta_t(n,t)) - F_n(n,t)\sin(\theta_t(n,t)), \\
F_y(t) &= \sum_{n=1}^{N} F_y(n,t), \\
F_z(t) &= \sum_{n=1}^{N} F_z(n,t).
\end{aligned} \tag{11}$$

E. MECHANICAL MANIPULATOR DYNAMICS

A multibody recursive formula [26] based on the joint coordinate system was used to improve the computational efficiency. The generalized coordinates, which describe the motion of the system, consist only of the linear or rotational motion at the joints. Thus, the equations of motion are simple and efficient calculation is possible. In addition, these equations can be easily extended to a multi DOF system.

The equations of motion for the hydraulic manipulator can be obtained by adding the hydraulic motor torque of (4), the friction force of (5), and the contact force of (11) to the dynamic model of the mechanical manipulator as follows:

$$\boldsymbol{M}(\boldsymbol{q}(t))\ddot{\boldsymbol{q}}(t) = \boldsymbol{Q}(\dot{\boldsymbol{q}}(t), \boldsymbol{q}(t)) - \boldsymbol{Q}_f(\dot{\boldsymbol{q}}(t)) + \boldsymbol{\tau}_m(\dot{\boldsymbol{q}}(t), \boldsymbol{u}(t)), \tag{12}$$

where $\boldsymbol{q} \in \Re^{6\times 1}$ is the joint position vector, $\boldsymbol{u} \in \Re^{6\times 1}$ is the control input vector, $\boldsymbol{M} \in \Re^{6\times 6}$ is the generalized inertia matrix, $\boldsymbol{Q} \in \Re^{6\times 1}$ is the generalized force vector including Coriolis, gravity, and contact force, $\boldsymbol{Q}_f \in \Re^{6\times 1}$ is the joint friction vector, and $\boldsymbol{\tau}_m$ is the hydraulic motor torque vector.

The contact force obtained through (11) is automatically included in the generalized force term ($\boldsymbol{Q}$) by recursive formula.

III. NUMERICAL INTEGRATION ALGORITHM

The hydraulic manipulator has a stiff characteristic due to the compressibility of the fluid. Implicit integration algorithms are widely used for real-time simulations of stiff systems. These methods can satisfy both the accuracy of the solution and real-time performance by using a numerical damping effect. We considered a noniterative implicit integration algorithm based on the HHT-α method [28] to guarantee real-time performance. This method is advantageous for real-time simulations because it is robust without an iterative method. For the hydraulic manipulator, the noniterative HHT-α was applied to the servo valve dynamics, hydraulic equations, and mechanical manipulator dynamics.

A. SERVO VALVE STATE

The modified servo valve dynamics applying numerical damping effect (α) to (1) is defined as follows:

$$\begin{aligned}
&\ddot{x}^i_{v,n+1} + (1+\alpha)(2\zeta_v\omega_{n_v}\dot{x}^i_{v,n+1} + \omega^2_{n_v}x^i_{v,n+1} - \omega^2_{n_v}K^i_{sv}u^i_{n+1}) \\
&\quad -\alpha(2\zeta_v\omega_{n_v}\dot{x}^i_{v,n} + \omega^2_{n_v}x^i_{v,n} - \omega^2_{n_v}K^i_{sv}u^i_n) = 0,
\end{aligned} \tag{13}$$

where $(\cdot)_{n+1}$ means the current step, $(\cdot)_n$ denotes the previous step, and α is the numerical damping effect that satisfies the condition of $-1/3 \le \alpha \le 0$.

The modified servo valve dynamics can be linearized using the noniterative HHT-α method as follows:

$$\begin{aligned}
&\left[\left(\omega^2_{n_v}\right)^{-1} - \beta h^2 J^i_{x_{v,n}} - \gamma h J^i_{\dot{x}_{v,n}}\right]\Delta\dot{x}^i_{v,n} \\
&\quad = h\left[\omega^2_{n_v}K^i_{sv}u^i_n - 2\zeta^i_v\omega^i_{n_v}\dot{x}^i_{v,n} - \omega^2_{n_v}x^i_{v,n}\right] \\
&\qquad + h\left[\gamma h J^i_{x_{v,n}}\left(\dot{x}^i_{v,n} + \frac{h}{2}\left(1 - \frac{2\beta}{\gamma}\right)\ddot{x}^i_{v,n}\right)\right],
\end{aligned} \tag{14}$$

where $\beta = (1-\alpha)^2/4$ and $\gamma = (1-2\alpha)/2$ are integral coefficients associated with the numerical damping effect, h is the integral step size, and $J_{x_{v,n}}$ and $J_{\dot{x}_{v,n}}$ are system Jacobians with respect to the displacement and velocity of the spool, respectively. The detailed expressions are shown in (15).

$$\begin{aligned}
J^i_{x_{v,n}} &= -(1+\alpha)\omega^2_{n_v}, \\
J^i_{\dot{x}_{v,n}} &= -(1+\alpha)2\zeta_v\omega_{n_v}.
\end{aligned} \tag{15}$$

The displacement, velocity, and acceleration of the spool at the current step can be obtained using (14).

$$\begin{aligned}
x^i_{v,n+1} &= x^i_{v,n} + h\left[\dot{x}^i_{v,n} + \frac{h}{2}\left(1 - \frac{2\beta}{\gamma}\right)\ddot{x}^i_{v,n} + \frac{\beta}{\gamma}\Delta\dot{x}^i_{v,n}\right], \\
\dot{x}^i_{v,n+1} &= \dot{x}^i_{v,n} + \Delta\dot{x}^i_{v,n}, \\
\ddot{x}^i_{v,n+1} &= \ddot{x}^i_{v,n} + \frac{1}{\gamma}\left(\frac{1}{h}\Delta\dot{x}^i_{v,n} - \ddot{x}^i_{v,n}\right).
\end{aligned} \tag{16}$$

B. HYDRAULIC STATE

The hydraulic equations of (3) can also be redefined by applying the numerical damping effect as follows:

$$\begin{aligned}
&\dot{P}^i_{1,n+1} - (1+\alpha)\frac{\beta_e}{V^i_{1,n+1}}\left[Q^i_{1,n+1} - Q^i_{leak,n+1} - \dot{V}^i_{1,n+1}\right] \\
&\quad +\alpha\frac{\beta_e}{V^i_{1,n+1}}\left[Q^i_{1,n} - Q^i_{leak,n} - \dot{V}^i_{1,n}\right] = 0, \\
&\dot{P}^i_{2,n+1} - (1+\alpha)\frac{\beta_e}{V^i_{2,n+1}}\left[Q^i_{2,n+1} + Q^i_{leak,n+1} - \dot{V}^i_{2,n+1}\right] \\
&\quad +\alpha\frac{\beta_e}{V^i_{2,n+1}}\left[Q^i_{2,n} + Q^i_{leak,n} - \dot{V}^i_{2,n}\right] = 0.
\end{aligned} \tag{17}$$

The linearization of (17) is shown in (18).

$$\begin{aligned}
\left[1 - \gamma h J^i_{P_{1,n}}\right]\Delta P^i_{1,n} &= h\frac{\beta_e}{V^i_{1,n+1}}\left[Q^i_{1,n} - Q^i_{leak,n} - \dot{V}^i_{1,n}\right], \\
\left[1 - \gamma h J^i_{P_{2,n}}\right]\Delta P^i_{2,n} &= h\frac{\beta_e}{V^i_{2,n+1}}\left[Q^i_{2,n} + Q^i_{leak,n} - \dot{V}^i_{2,n}\right],
\end{aligned} \tag{18}$$

where $J_{P_{1,n}}$ and $J_{P_{2,n}}$ are system Jacobians with respect to the pressure at the supply and return ports. They are expressed as

$$\begin{aligned}
J^i_{P_{1,n}} &= (1+\alpha)\frac{\beta_e}{V^i_{1,n+1}}\frac{\partial Q^i_{1,n}}{\partial P^i_{1,n}}, \\
J^i_{P_{2,n}} &= (1+\alpha)\frac{\beta_e}{V^i_{2,n+1}}\frac{\partial Q^i_{2,n}}{\partial P^i_{2,n}}, \\
\frac{\partial Q^i_{1,n}}{\partial P^i_{1,n}} &= \begin{cases} -\frac{C^i_d x^i_{v,n}}{2\sqrt{\left|P_s - P^i_{1,n}\right|}} & \text{if } \left|x^i_{v,n}\right| \geq 0 \\ \frac{C^i_d x^i_{v,n}}{2\sqrt{\left|P^i_{1,n}\right|}} & \text{otherwise,} \end{cases} \\
\frac{\partial Q^i_{2,n}}{\partial P^i_{2,n}} &= \begin{cases} -\frac{C^i_d x^i_{v,n}}{2\sqrt{\left|P^i_{2,n}\right|}} & \text{if } \left|x^i_{v,n}\right| \geq 0 \\ \frac{C^i_d x^i_{v,n}}{2\sqrt{\left|P_s - P^i_{1,n}\right|}} & \text{otherwise.} \end{cases}
\end{aligned} \tag{19}$$

The pressure at the supply and return ports of the hydraulic motor can be obtained using (18) as follows:

$$\begin{aligned}
P^i_{1,n+1} &= P^i_{1,n} + \Delta P^i_{1,n}, \\
P^i_{2,n+1} &= P^i_{2,n} + \Delta P^i_{2,n}.
\end{aligned} \tag{20}$$

C. FRICTION STATE

We applied the numerical damping effect to the joint friction model of (5), as follows:

$$\begin{aligned}
&\dot{z}^j_{n+1} - (1+\alpha)\left[\dot{q}^j_{n+1} - \frac{\left|\dot{q}^j_{n+1}\right|}{g(\dot{q}^j_{n+1})}z^j_{n+1}\right] \\
&\quad +\alpha\left[\dot{q}^j_n - \frac{\left|\dot{q}^j_n\right|}{g(\dot{q}^j_n)}z^j_n\right] = 0.
\end{aligned} \tag{21}$$

The linearized equation of (21) can be expressed as

$$\left[1 - \gamma h J^j_{z_n}\right]\Delta z^j_n = h\left[\dot{q}^j_n - \frac{\left|\dot{q}^j_n\right|}{g(\dot{q}^j_n)}z^j_n\right], \tag{22}$$

where J_{z_n} is a system Jacobian with respect to z_n. The detailed expression is shown below:

$$J^j_{z_n} = -(1+\alpha)\frac{\left|\dot{q}^j_n\right|}{g(\dot{q}^j_n)}. \tag{23}$$

We estimated the average deflection of the bristles at the current step using (22).

$$z^j_{n+1} = z^j_n + \Delta z^j_n. \tag{24}$$

D. MECHANICAL MANIPULATOR STATE

Finally, the numerical damping effect can be applied to the hydraulic manipulator dynamics of (12) as follows:

$$\begin{aligned}
&\boldsymbol{M}(\boldsymbol{q}_{n+1})\ddot{\boldsymbol{q}}_{n+1} - (1+\alpha) \\
&\quad \times\left[\boldsymbol{Q}(\dot{\boldsymbol{q}}_{n+1}, \boldsymbol{q}_{n+1}) - \boldsymbol{Q}_f(\dot{\boldsymbol{q}}_{n+1}) + \boldsymbol{\tau}_m(\dot{\boldsymbol{q}}_{n+1})\right] \\
&\quad +\alpha\left[\boldsymbol{Q}(\dot{\boldsymbol{q}}_n, \boldsymbol{q}_n) - \boldsymbol{Q}_f(\dot{\boldsymbol{q}}_n) + \boldsymbol{\tau}_m(\dot{\boldsymbol{q}}_n)\right] = \boldsymbol{0}.
\end{aligned} \tag{25}$$

Equation (25) can be linearized as follows:

$$\begin{aligned}
&\left[\boldsymbol{M}(\boldsymbol{q}_n) - \beta h^2 \boldsymbol{J}_{\boldsymbol{q}_n} - \gamma h \boldsymbol{J}_{\dot{\boldsymbol{q}}_n}\right]\Delta\dot{\boldsymbol{q}}_n \\
&\quad = h\left[\boldsymbol{Q}(\dot{\boldsymbol{q}}_n, \boldsymbol{q}_n) - \boldsymbol{Q}_f(\dot{\boldsymbol{q}}_n) + \boldsymbol{\tau}_m(\dot{\boldsymbol{q}}_n)\right] \\
&\quad\quad +h\left[\gamma h \boldsymbol{J}_{\boldsymbol{q}_n}\left(\dot{\boldsymbol{q}}_n + \frac{h}{2}\left(1 - \frac{2\beta}{\gamma}\right)\ddot{\boldsymbol{q}}_n\right)\right],
\end{aligned} \tag{26}$$

where $\boldsymbol{J}_{\boldsymbol{q}_n} \in \Re^{6\times 6}$ and $\boldsymbol{J}_{\dot{\boldsymbol{q}}_n} \in \Re^{6\times 6}$ are system Jacobian matrices with respect to the position and velocity of the joint for the hydraulic manipulator, respectively. The detailed expressions are shown below:

$$\begin{aligned}
\boldsymbol{J}_{\boldsymbol{q}_n} &= (1+\alpha)\frac{\partial \boldsymbol{Q}(\dot{\boldsymbol{q}}_n, \boldsymbol{q}_n)}{\partial \boldsymbol{q}_n} - \frac{\partial \boldsymbol{M}(\boldsymbol{q}_n)}{\partial \boldsymbol{q}_n}, \\
\boldsymbol{J}_{\dot{\boldsymbol{q}}_n} &= (1+\alpha)\left[\frac{\partial \boldsymbol{Q}(\dot{\boldsymbol{q}}_n, \boldsymbol{q}_n)}{\partial \dot{\boldsymbol{q}}_n} - \frac{\partial \boldsymbol{Q}_f(\dot{\boldsymbol{q}}_n)}{\partial \dot{\boldsymbol{q}}_n}\right].
\end{aligned} \tag{27}$$

The position, velocity, and acceleration of the joint at the current step can be obtained as follows:

$$\begin{aligned}
\boldsymbol{q}_{n+1} &= \boldsymbol{q}_n + h\left[\dot{\boldsymbol{q}}_n + \frac{h}{2}\left(1 - \frac{2\beta}{\gamma}\right)\ddot{\boldsymbol{q}}_n + \frac{\beta}{\gamma}\Delta\dot{\boldsymbol{q}}_n\right], \\
\dot{\boldsymbol{q}}_{n+1} &= \dot{\boldsymbol{q}}_n + \Delta\dot{\boldsymbol{q}}_n, \\
\ddot{\boldsymbol{q}}_{n+1} &= \ddot{\boldsymbol{q}}_n + \frac{1}{\gamma}\left(\frac{1}{h}\Delta\dot{\boldsymbol{q}}_n - \ddot{\boldsymbol{q}}_n\right).
\end{aligned} \tag{28}$$

The overall integration process is shown in Fig. 5.

IV. NUMERICAL SIMULATIONS

A. VALIDATION OF OPEN-LOOP RESPONSES

We verified the accuracy of the hydraulic manipulator model through an open-loop control test. The control input of (29) was applied to each servo valve, and the actual experiment

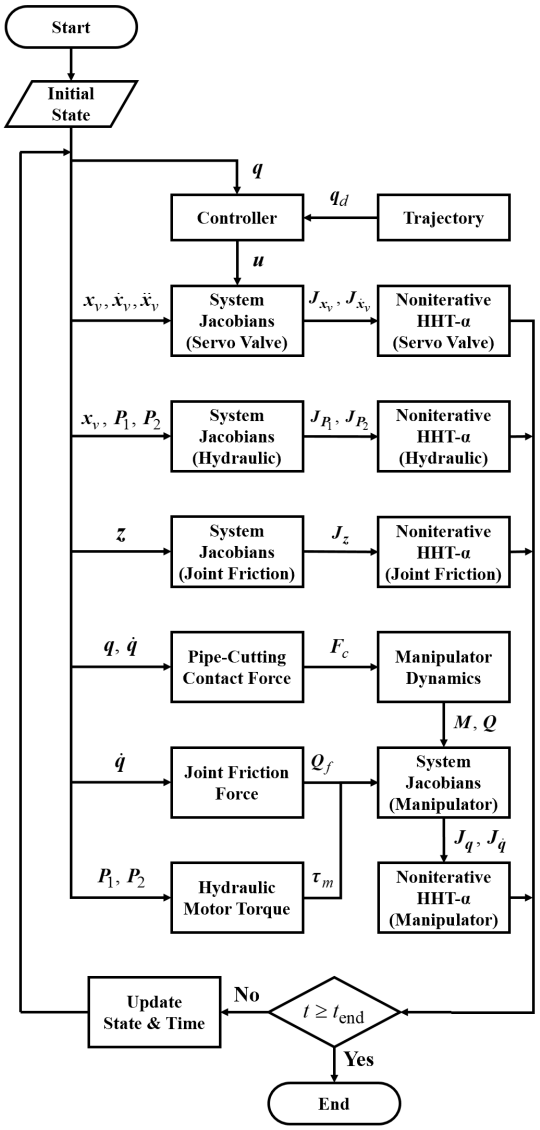

FIGURE 5. Computational flow chart.

and simulation were compared. Only one servo valve was operated sequentially, and the others were fixed.

$$u^i(t) = 10 \sin(\pi t) \text{ mA}. \tag{29}$$

The comparison results are shown in Fig. 6. The solid blue line is the experimental result, and the dash-dot red line is the simulation result. In the experiments, actual joint positions were measured using resolver sensors at the individual joints of the hydraulic manipulator. For the second joint, which is a prismatic joint, the displacement value was converted from the rotation value of the resolver sensor owing to the ball screw mechanism. The simulation results are similar to the experimental results for all joints, and the simulation error is less than 0.4 deg and 0.3 mm. Therefore, the implemented hydraulic manipulator dynamics can well describe the characteristics of the actual system.

TABLE 4. Gain Properties for circular trajectory-tracking simulation.

Gain	Joint 1	Joint 2	Joint 3	Joint 4	Joint 5	Joint 6
K_d	0.04	0.10	0.05	0.04	0.10	0.10
K_p	1.28	3.20	1.60	1.28	3.20	3.20
K_i	2.56	6.40	3.20	2.56	6.40	6.40

TABLE 5. Computational efficiency for circular trajectory-tracking simulation.

Integration method	Integral step size	Computational time
Runge-Kutta 4^{th}	0.02 ms	154.443 s
Adams-Bashforth 3^{rd}	0.02 ms	48.066 s
Noniterative HHT-α	0.2 ms	38.544 s

B. TRAJECTORY-TRACKING SIMULATION

A trajectory-tracking simulation was performed to test the integrated simulation with the controller. We assumed that the end-effector of the hydraulic manipulator follows the circular trajectory in Cartesian space. The target trajectory was designed with a radius of 300 mm, and the servo valves were controlled to follow with a velocity of 7.5 deg/s, as shown in Fig. 7.

The PID controller using systematic gain selection method [29] was used to control of the servo valves. This method can easily improve the robustness for nonlinear systems. The control input is defined as follows:

$$\boldsymbol{u}(t) = \boldsymbol{K}_d \dot{\boldsymbol{e}}(t) + \boldsymbol{K}_p \boldsymbol{e}(t) + \boldsymbol{K}_i \int \boldsymbol{e}(\tau) d\tau, \tag{30}$$

where $\boldsymbol{e} = \boldsymbol{q}_d - \boldsymbol{q} \in \Re^{6\times1}$ is the joint position error vector, $\boldsymbol{q}_d \in \Re^{6\times1}$ is the desired joint position vector from the trajectory, $\boldsymbol{K}_d \in \Re^{6\times6}$ is the diagonal matrix of the differential gain, $\boldsymbol{K}_p \in \Re^{6\times6}$ is the diagonal matrix of the proportional gain, and $\boldsymbol{K}_i \in \Re^{6\times6}$ is the diagonal matrix of the integral gain. The gain properties for circular trajectory-tracking simulation are summarized in Table 4.

The control frequency is 100 Hz, and the integral computation frequency is 5 kHz. If the integral calculation is slower than 5 kHz, the accuracy of the solution will be decreased significantly. The results of circular trajectory-tracking simulation are shown in Fig. 8. The solid blue line is the target circular trajectory, and the dash-dot red line is the position of the end-effector. The tracking root-mean-square (RMS) error of each axis was 0.4963, 0.1705, and 0.6564 mm for the X-, Y-, and Z-axes, respectively. The trajectory of the hydraulic manipulator's end-effector matched the target circular trajectory. The above results are similar to the experimental results under the conditions considered in [30]. Thus, even for closed-loop control simulation, simulation results that agree with the results of the actual system can be obtained.

In addition, we measured the computational time to verify real-time performance. The PC used for simulation has specifications of Intel(R) Core(TM) i7-9750H CPU @ 2.60 GHz and 32GB RAM. The computational time should be faster than the total simulation time of 60 s. The efficiency of the noniterative HHT-α method was proved by comparing with

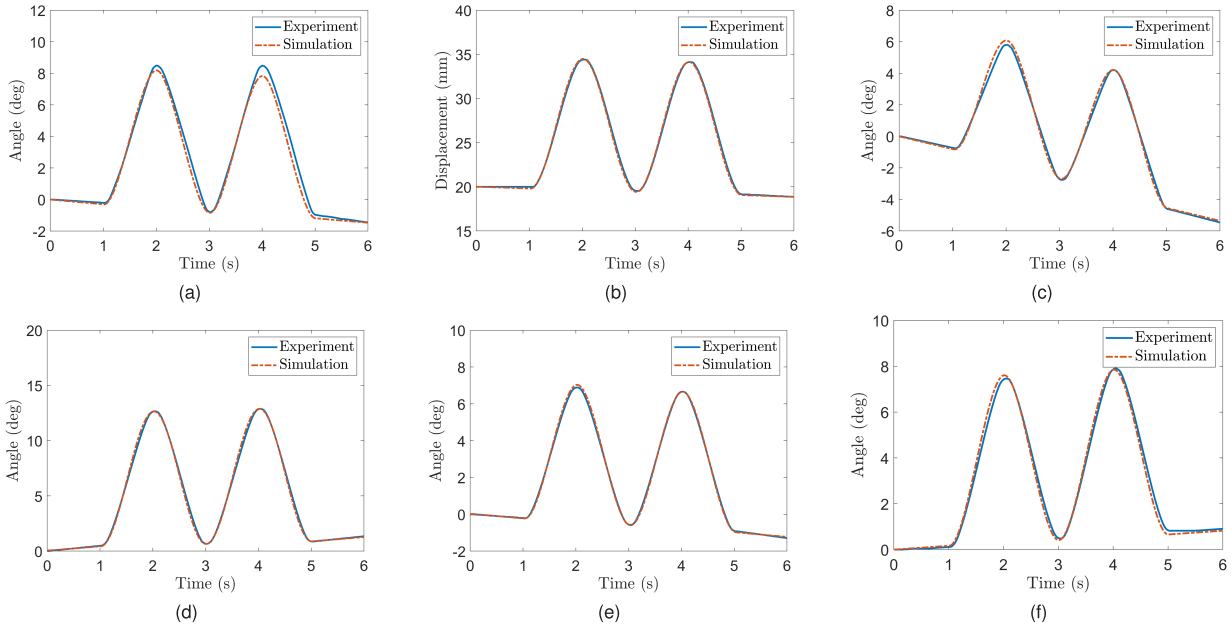

FIGURE 6. Open-loop control test results. (a), (b), (c), (d), (e), and (f) are showing position of joint 1, 2, 3, 4, 5, and 6, respectively.

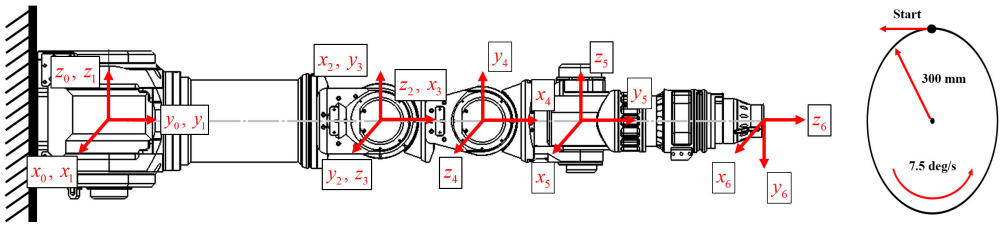

FIGURE 7. Configuration of the circular trajectory-tracking simulation.

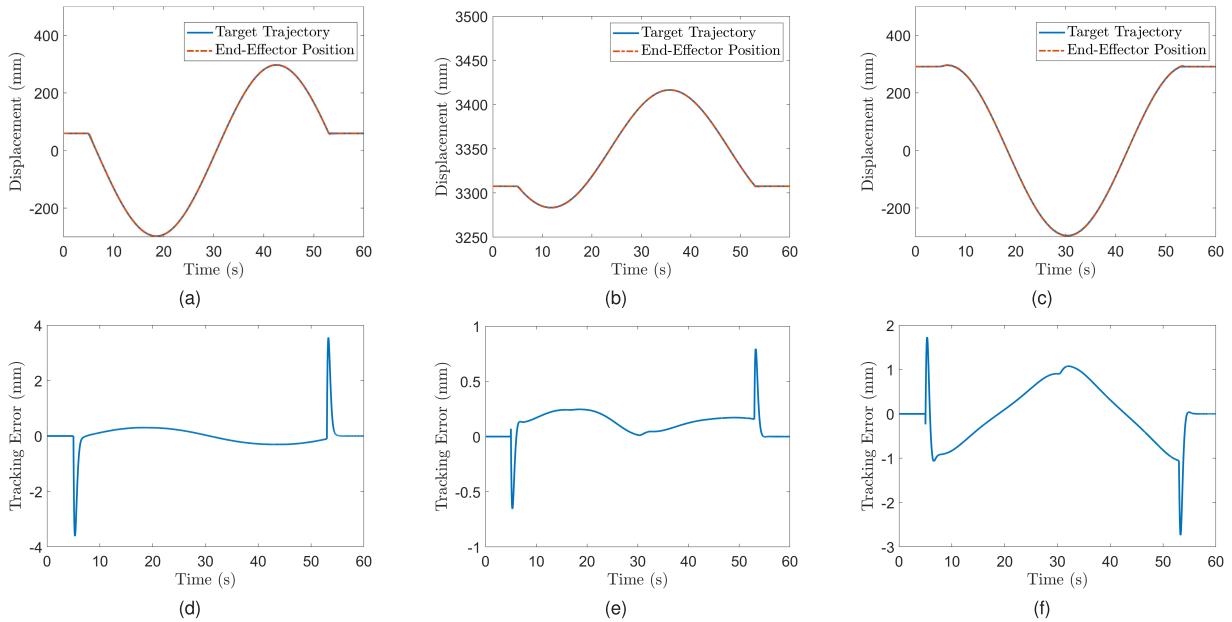

FIGURE 8. Simulation results of circular trajectory-tracking. (a), (b), and (c) are showing position of the end-effector for the X-, Y-, and Z-axes, respectively. (d), (e), and (f) are showing tracking error for the X-, Y-, and Z-axes, respectively.

Runge-Kutta 4^{th} order and Adams-Bashforth 3^{rd} order methods, which are widely used for simulation, as summarized in Table 5. The Runge-Kutta 4^{th} order method is not suitable for real-time simulations because it requires more computational

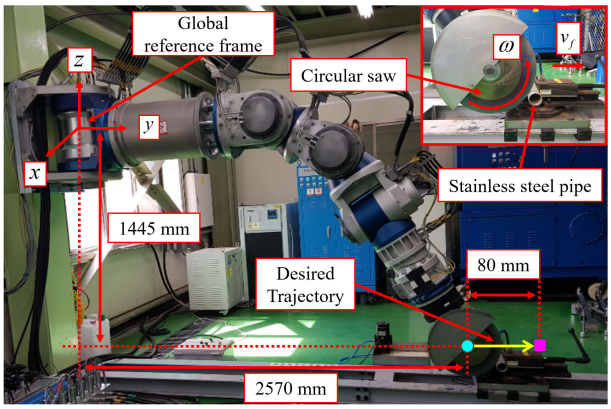

FIGURE 9. Configuration of the pipe-cutting simulation. A cyan circle point means an initial position and a magenta square dot denotes a target position.

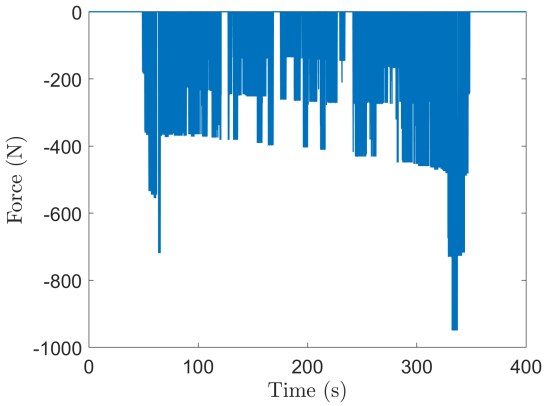

FIGURE 10. Cutting force during pipe-cutting.

time than the total simulation time. The Adams-Bashforth 3^{rd} order and noniterative HHT-α method can be used for real-time simulations. In particular, the noniterative HHT-α method can perform real-time simulation while maintaining the solution's accuracy even if the integral step size is increased ten times. Therefore, the advanced simulation with the controller is possible, and the performance of the control system can be evaluated in real-time using a developed simulator.

C. PIPE-CUTTING SIMULATION

We performed a real-time simulation of pipe-cutting considering the contact force. The configuration of pipe-cutting is shown in Fig. 9. The cutting tool used a circular saw and was attached to the end-effector of the hydraulic manipulator. The pipe was cut by controlling the center of the circular saw following the cutting trajectory. The circular saw rotated at an angular velocity (ω) of 30 rpm, and the cutting tool moved 80 mm with respect to the positive Y-axis with a feed rate (v_f) of 12 mm/min. The initial position of Y-axis was 2570 mm. In addition, the position of X- and Z-axes were fixed as 0 mm and -1445 mm, respectively.

The contact force obtained through the pipe-cutting contact model is shown in Fig. 10. Pipe-cutting started at 50 s and completed at 350 s. The magnitude of the cutting force was determined from the shear stress (τ_s) of the target material, as shown in (9). For stainless steel, the range of shear stress was 320-880 MPa. We assumed a large cutting force and considered the maximum shear stress. Thus, while cutting stainless steel pipe, a large cutting force is applied to the hydraulic manipulator.

In Fig. 10, the contact force was significantly increased at the beginning of cutting. After the breakthrough the inner diameter of the pipe, the contact force was decreased. In the final process of cutting, the circular saw and the pipe were recontacted, and the contact force was increased again. Thus, the physical phenomenon was well implemented during pipe-cutting.

TABLE 6. Gain Properties for pipe-cutting simulation.

Gain	Joint 1	Joint 2	Joint 3	Joint 4	Joint 5	Joint 6
K_d	0.020	0.050	0.025	0.020	0.050	0.050
K_p	0.640	1.600	0.800	0.640	1.600	1.600
K_i	1.280	3.200	1.600	1.280	3.200	3.200

The results of the pipe-cutting simulation are shown in Fig. 11. The solid blue line is the target circular trajectory, and the dash-dot red line is the position of the circular saw's center. The gain properties for pipe-cutting simulation are summarized in Table 6. Same as trajectory-tracking simulation, the control frequency was 100 Hz, and the integral computation frequency was 5 kHz. The tracking RMS error of each axis was 0.0013, 0.0146, and 0.0071 mm for the X-, Y-, and Z-axes, respectively. The magnitude of the tracking error increased with the contact force at the start of the cut. After cutting to reach the inner diameter of the pipe, the tracking error also reduced because the contact area decreased. At the end of the cut, the tracking error increased as the contact force increased again. Thus, the actual environment such as vibration was well represented in the simulation.

The computational time was also measured to verify real-time performance, as summarized in Table 7. The integral step size of Runge-Kutta 4^{th} order and Adams-Bashforth 3^{rd} order method was reduced due to the addition of the cutting force, and the real-time performance was not satisfied. They required more computational time than of 400 s to the pipe-cutting simulation. The real-time simulation including the contact force was only possible with the noniterative HHT-α method because the computational time is faster than the total simulation time. Thus, robust numerical integration algorithms should be applied for the real-time integrated control simulation considering contact situations.

Thus, the real-time simulation of pipe-cutting with the hydraulic manipulator is possible using the proposed simulator. Based on numerical simulations, the proposed simulator can be applied for the cutting of larger and heavier objects.

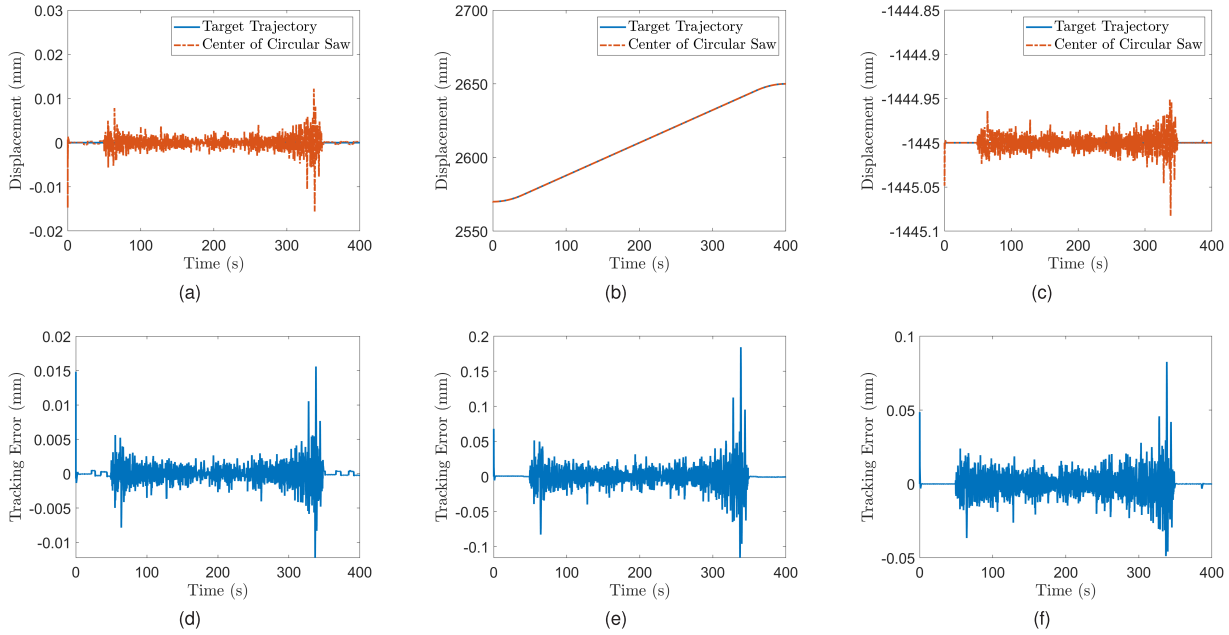

FIGURE 11. Simulation results of pipe-cutting. (a), (b), and (c) are showing position of the end-effector for the X-, Y-, and Z-axes, respectively. (d), (e), and (f) are showing tracking error for the X-, Y-, and Z-axes, respectively.

TABLE 7. Computational efficiency for pipe-cutting simulation.

Integration method	Integral step size	Computational time
Runge-Kutta 4^{th}	0.01 ms	2139.93 s
Adams-Bashforth 3^{rd}	0.01 ms	583.493 s
Noniterative HHT-α	0.2 ms	273.882 s

V. CONCLUSION

In this paper, we proposed a real-time simulator of a six DOF hydraulic manipulator. The advantages of the proposed simulator are that the advanced simulation is possible with real-time data, and the working environment is considered. We applied a multibody recursive formula coupled with the hydraulic equations and noniterative integration algorithm to achieve real-time performance. The pipe-cutting model was also added to simulate working scenarios. The performance of the developed real-time simulator was verified to be similar to that of the real system through an open-loop control experiment. The real-time performance was demonstrated via the integrated simulation with the controller for trajectory-tracking and pipe-cutting. The results of numerical simulations establish excellent accuracy of the proposed real-time simulator without model simplification and demonstrate the simulation of pipe-cutting in real-time using the numerical integration algorithm.

Moreover, the proposed real-time simulator can be applied to hardware-in-the-loop simulation (HILS) or teleoperation simulation, which include actual hardware like haptic master device and electronic control unit (ECU). Thus, the developed real-time simulator is useful for the design of mechanical parts, control performance evaluation, scenario validation, and operator training. For future studies, we aim to add a master-slave teleoperation algorithm and extend it to the digital twin.

REFERENCES

[1] S. Sivčev, J. Coleman, E. Omerdić, G. Dooly, and D. Toal, "Underwater manipulators: A review," *Ocean Eng.*, vol. 163, no. 1, pp. 431–450, Sep. 2018.

[2] C. Semini, V. Barasuol, J. Goldsmith, M. Frigerio, M. Focchi, Y. Gao, and D. G. Caldwell, "Design of the hydraulically actuated, torque-controlled quadruped robot HyQ2Max," *IEEE/ASME Trans. Mechatronics*, vol. 22, no. 2, pp. 635–646, Apr. 2016.

[3] S. Kuindersma, R. Deits, M. Fallon, A. Valenzuela, H. Dai, F. Permenter, T. Koolen, P. Marion, and R. Tedrake, "Optimization-based locomotion planning, estimation, and control design for the atlas humanoid robot," *Auton. Robots*, vol. 40, no. 3, pp. 429–455, Mar. 2016.

[4] M. J. Bakari, K. M. Zied, and D. W. Seward, "Development of a multi-arm mobile robot for nuclear decommissioning tasks," *Int. J. Adv. Robot. Syst.*, vol. 4, no. 4, pp. 387–406, Dec. 2007.

[5] O. David, Y. Measson, C. Bidard, C. Rotinat-Libersa, and F. Russotto, "MAESTRO: A hydraulic manipulator for maintenance and decommissioning application," in *Proc. Trans. Eur. Nucl. Cong.*, 2007, pp. 547–554.

[6] C. Chabal and Y. Soulabaille, "Virtual Reality: A way to prepare and optimize operations in decommissioning projects," in *Proc. Int. Symp. PREDEC*, 2016, pp. 2–10.

[7] F. Tao, H. Zhang, A. Liu, and A. Y. Nee, "Digital twin in industry: State-of-the-art," *IEEE Trans. Ind. Informat.*, vol. 15, no. 4, pp. 2405–2415, Apr. 2018.

[8] A. Fuller, Z. Fan, C. Day, and C. Barlow, "Digital twin: Enabling technologies, challenges and open research," *IEEE Access*, vol. 8, pp. 108952–108971, 2020.

[9] Q. Qi and F. Tao, "Digital twin and big data towards smart manufacturing and Industry 4.0: 360 degree comparison," *IEEE Access*, vol. 6, pp. 3585–3593, 2018.

[10] J. Collins, S. Chand, A. Vanderkop, and D. Howard, "A review of physics simulators for robotic applications," *IEEE Access*, vol. 9, pp. 51416–51431, 2021.

[11] H. Roozbahani, M. Alizadeh, A. Ahomäki, and H. Handroos, "Coordinate-based control for a materials handling equipment utilizing real-time simulation," *Autom. Construct.*, vol. 122, Feb. 2021, Art. no. 103483.

[12] E. Papadopoulos and Y. Gonthier, "On the development of a real-time simulator engine for a hydraulic forestry machine," *Int. J. Fluid Power*, vol. 3, no. 1, pp. 55–65, Jan. 2002.
[13] H. Zhao and M. Kawai, "Compensation of hydraulic drag for an underwater manipulator using a real-time SPH fluid simulator: Application in a master-slave tele-operation," in *Proc. 2nd Int. Congr. Comput. Appl. Comput. Sci.*, 2012, pp. 29–38.
[14] J. A. Ferreira, A. F. Quintã, and C. M. Cabral, "Hardware-in-the-loop simulation experiments with a hydraulic manipulator model," *Austral. J. Mech. Eng.*, vol. 2, no. 2, pp. 125–132, Jan. 2005.
[15] C.-G. Park, S. Yoo, H. Ahn, J. Kim, and D. Shin, "A coupled hydraulic and mechanical system simulation for hydraulic excavators," *Proc. Inst. Mech. Eng., I, J. Syst. Control Eng.*, vol. 234, no. 4, pp. 527–549, Apr. 2020.
[16] J. A. Ferreira, F. G. Almeida, M. R. Quintas, and J. P. E. de Oliveira, "Hybrid models for hardware-in-the-loop simulation of hydraulic systems Part 2: Experiments," *Proc. Inst. Mech. Eng., I, J. Syst. Control Eng.*, vol. 218, no. 6, pp. 475–486, Sep. 2004.
[17] Y. Zhang, W. Ding, and H. Deng, "Reduced dynamic modeling for heavy-duty hydraulic manipulators with multi-closed-loop mechanisms," *IEEE Access*, vol. 8, pp. 101708–101720, 2020.
[18] M. E. Baharudin, A. Rouvinen, P. Korkealaakso, and A. Mikkola, "Real-time multibody application for tree harvester truck simulator," *Proc. Inst. Mech. Eng. K, J. Multi-Body Dyn.*, vol. 228, no. 2, pp. 182–198, Jun. 2014.
[19] E. Hairer, S. P. Nørsett, and G. Wanner, *Solving Ordinary Differential Equations. 1, Nonstiff Problems*. Berlin, Germany: Springer, 1993.
[20] M. Liu, W. Cao, and Z. Fan, "Convergence and stability of the semi-implicit Euler method for a linear stochastic differential delay equation," *J. Comput. Appl. Math.*, vol. 170, no. 2, pp. 255–268, Sep. 2004.
[21] G. Rill, "A modified implicit Euler algorithm for solving vehicle dynamic equations," *Multibody Syst. Dyn.*, vol. 15, no. 1, pp. 1–24, Feb. 2006.
[22] M. Arnold, B. Burgermeister, and A. Eichberger, "Linearly implicit time integration methods in real-time applications: DAEs and stiff ODEs," *Multibody Syst. Dyn.*, vol. 17, nos. 2–3, pp. 99–117, Feb. 2007.
[23] H. M. Hilber, T. J. R. Hughes, and R. L. Taylor, "Improved numerical dissipation for time integration algorithms in structural dynamics," *Earthquake Eng. Struct. Dyn.*, vol. 5, no. 3, pp. 283–292, Sep. 1977.
[24] D. Negrut, R. Rampalli, G. Ottarsson, and A. Sajdak, "On an implementation of the Hilber-Hughes-Taylor method in the context of index 3 differential-algebraic equations of multibody dynamics (DETC2005-85096)," *J. Comput. Nonlinear Dyn.*, vol. 2, no. 1, pp. 73–85, Jan. 2007.
[25] J. Wang and Z. Li, "Implementation of HHT algorithm for numerical integration of multibody dynamics with holonomic constraints," *Nonlinear Dyn.*, vol. 80, nos. 1–2, pp. 817–825, Jan. 2015.
[26] F.-F. Tsai and E. J. Haug, "Real-time multibody system dynamic simulation: Part I. A modified recursive formulation and topological analysis," *Mech. Struct. Mach.*, vol. 19, no. 1, pp. 99–127, Jan. 1991.
[27] C. C. de Wit, H. Olsson, K. J. Åström, and P. Lischinsky, "A new model for control of systems with friction," *IEEE Trans. Autom. Control*, vol. 40, no. 3, pp. 419–425, Mar. 1995.
[28] M. Kim, H. Song, and S.-S. Kim, "A non-iterative implicit integration method using a HHT-α integrator for real-time analysis of multibody systems," *J. Mech. Sci. Technol.*, vol. 33, no. 3, pp. 1087–1096, Mar. 2019.
[29] P. H. Chang and J. H. Jung, "A systematic method for gain selection of robust PID control for nonlinear plants of second-order controller canonical form," *IEEE Trans. Control Syst. Technol.*, vol. 17, no. 2, pp. 473–483, Mar. 2008.
[30] M. Kim and S.-U. Lee, "PID with a switching action controller for nonlinear systems of second-order controller canonical form," *Int. J. Control, Autom. Syst.*, vol. 19, no. 7, pp. 2343–2356, Mar. 2021.
[31] H. E. Merritt, *Hydraulic Control Systems*. Hoboken, NJ, USA: Wiley, 1991.
[32] Y. Kordestany and Y. Ma, "Force calculation using analytical and CAE methods for thin-blade slotting process," *Cogent Eng.*, vol. 4, no. 1, Dec. 2017, Art. no. 1412106.

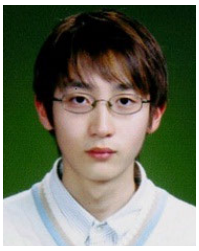

MYOUNGHO KIM (Member, IEEE) received the B.S., M.S., and Ph.D. degrees from the Department of Mechatronics Engineering, Chungnam National University, Daejeon, South Korea, in 2011, 2013, and 2020, respectively.

Since 2013, he has been a Postdoctoral Researcher with the Nuclear Robot Division, Korea Atomic Energy Research Institute (KAERI), Daejeon. His research interests include robotics, dynamics and control, hydraulic systems, master-slave teleoperation, modeling and simulation, real-time analysis, and digital twin.

SUNG-UK LEE (Member, IEEE) received the B.S. degree in precision engineering and the M.S. and Ph.D. degrees in mechanical engineering from the Korea Advanced Institute of Science and Technology (KAIST), Daejeon, South Korea, in 1993, 1995, and 2002, respectively.

He is currently a Principal Researcher with the Nuclear Robot Division, KAERI, Daejeon. His research interests include nuclear robotics, teleoperation, and nonlinear control algorithms.

SUNG-SOO KIM received the Ph.D. degree in mechanical engineering from the University of Iowa, USA, in 1988.

He is currently a Professor with the Mechatronics Engineering Department, Chungnam National University, Daejeon, South Korea. His research interests include real-time multibody dynamics and its application to automotive systems and robot systems.